Volume 24
Number 34
14 September 2022
Pages 19979–20568

PCCP

Physical Chemistry Chemical Physics

rsc.li/pccp

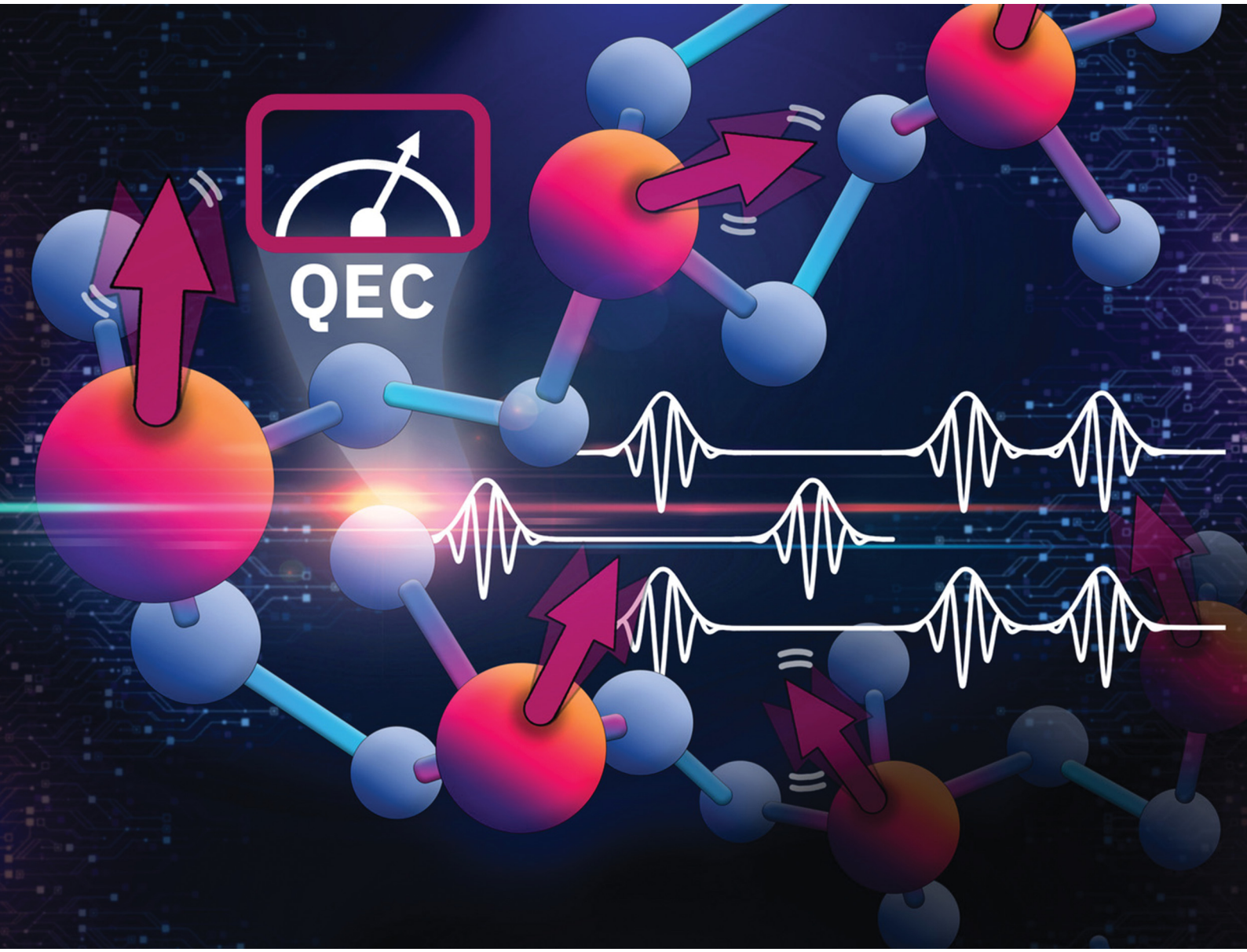

ISSN 1463-9076

ROYAL SOCIETY OF CHEMISTRY

PAPER
Paolo Santini *et al.*
Quantum error correction with molecular spin qudits

PCCP

ROYAL SOCIETY OF CHEMISTRY

PAPER

View Article Online
View Journal | View Issue

Cite this: *Phys. Chem. Chem. Phys.*, 2022, **24**, 20030

Quantum error correction with molecular spin qudits

Mario Chizzini, [ab] Luca Crippa, [ac] Luca Zaccardi, [ad] Emilio Macaluso, [abd] Stefano Carretta, [abd] Alessandro Chiesa [abd] and Paolo Santini *[abd]

Received 14th March 2022,
Accepted 6th June 2022

DOI: 10.1039/d2cp01228f

rsc.li/pccp

Thanks to the large number of levels which can be coherently manipulated, molecular spin systems constitute a very promising platform for quantum computing. Indeed, they can embed quantum error correction within single molecular objects, thus greatly simplifying its actual realization in the short term. We consider a recent proposal, which exploits a spin qudit to encode the protected unit, and is tailored to fight pure dephasing. Here we compare the implementation of this code on different molecules, in which the qudit is provided by either an electronic or a nuclear spin (S, $I > 1$), coupled to a spin-1/2 electronic ancilla for error detection. By thorough numerical simulations we show that a significant gain in the effective phase memory time can be achieved. This is further enhanced by exploiting pulse-shaping techniques to reduce the leakage and/or the impact of decoherence during correction. Moreover, we simulate the implementation of single-qubit operations on the encoded states.

1 Introduction

Open-shell molecular spin systems, either Molecular Nanomagnets (MNM)[1–13] or genuinely organic compounds,[14–17] are very promising units of a future quantum computing architecture. A prominent feature which makes MNMs more attractive than many other established platforms[18–26] (based on encoding and manipulating information on two level units called qubits) is represented by their intrinsic multi-level structure.[27] Indeed, these many low-energy and highly coherent levels,[5,28–30] easily accessible by electro-magnetic pulses,[31–33] can be exploited to encode information and design algorithms based on a multi-level (qudit) logic.[34–41]

In particular, MNMs can embed quantum-error correction (QEC) within a single molecular object, as opposed to standard implementations, where logical units are encoded into a large collection of qubits.[42,43] Note that, due to the intrinsic fragility of quantum system, the achievement of quantum error correction represents a crucial milestone towards the realization of a scalable quantum-computing architecture, able to outclass classical computers in the solution of a wide variety of problems. However, the great overhead of qubits and operations required to protect information *via* QEC makes the resulting register still intractable, even for the most advanced realizations. The complementary point of view offered by multi-level molecular spin systems would significantly facilitate the actual realization of error-protected quantum computing units.[13]

To achieve this goal, we have recently proposed a scheme which allows one to suppress the most important source of noise in molecular spin systems, represented by pure dephasing.[44–46] The proposal relies on the use of a spin $S > 1$ as the elementary logical unit of our quantum computer. Its $2S + 1$ energy levels, exceeding the number of two required to encode the logical states 0 and 1, provide the additional degrees of freedom needed to encode a protected state, such that errors can be identified and corrected. This detection is accomplished with the help of a spin 1/2 ancilla, which allows one to flag each error without corrupting the encoded logical state.

We present here an analysis of the performance of this code on different molecular platforms, based on realistic parameters. Although the implementation of a molecular quantum computer equipped with QEC is still a long-term goal, here we would like to trace a route towards the first proof-of-principle demonstrations of this scheme, focusing in particular on the chemical requirements and on pulse sequence design. The examined platforms consist of either an electronic or a nuclear spin qudit, coupled to an electronic spin 1/2 ancilla by exchange or hyperfine interactions. We perform numerical simulations including the full sequence of pulses that implement the code. We show how to improve its performance with the help of proper pulse-shaping techniques, such as the derivative removal by adiabatic gate (DRAG).[47,48] We show that this technique is particularly useful to reduce the duration of the sequence (and hence the effect of decoherence) without

[a] *Dipartimento di Scienze Matematiche, Università di Parma, Fisiche e Informatiche, I-43124 Parma, Italy. E-mail: paolo.santini@unipr.it*
[b] *INFN-Sezione di Milano-Bicocca, gruppo collegato di Parma, I-43124 Parma, Italy*
[c] *IBM Italia s.p.a., Circonvallazione Idroscalo, I-20090 Segrate, Italy*
[d] *UdR Parma, INSTM, I-43124 Parma, Italy*

inducing a relevant leakage to unwanted transitions. By combining these results, a significant enhancement in the effective phase memory time of the spin qudit can be achieved, compared to an 1/2 isolated spin.

Finally, we illustrate how to implement single-qubit rotations on the encoded states protected by QEC.

2 Methods

In what follows, we consider two different molecular spin systems. The first is an electronic spin dimer (referred to as (**e**) from now on), whose spin Hamiltonian is given by

$$H_e = \mu_B B_0(g_z S_z + g_z^A s_z^A) + D{S_z}^2 + \mathbf{S}\cdot\mathbf{J}\cdot\mathbf{s}^A. \quad (1)$$

where the first two terms describe the Zeeman interaction with an external magnetic field B_0 along z (μ_B is Bohr magneton), $S > 1$ and $s^A = 1/2$ are electronic spins interacting with each other *via* an exchange tensor **J**, and D is an axial zero-field splitting term.

The second system (called (**n**) hereafter) consists of a single magnetic ion, typically a transition metal, containing an electronic spin $s^A = 1/2$, coupled by hyperfine interaction to a magnetic nucleus $I > 1$. It is described by the following spin Hamiltonian:

$$H_n = B_0(g_N\mu_N I_z + g_z^A\mu_B s_z^A) + Q{I_z}^2 + \mathbf{I}\cdot\mathbf{A}\cdot\mathbf{s}^A, \quad (2)$$

where again the first term describes the interaction of the nuclear and electronic spins with a external field (μ_N is the nuclear magneton), Q is the nuclear quadrupole coupling and **A** is the hyperfine tensor. In the following, for simplicity we assume diagonal **A** and **J** tensors.

In both cases, we work in a weak coupling regime, in which the eigenstates of Hamiltonians (1,2) are practically factorized and can thus be labelled with the quantum numbers $|M, m\rangle$, *i.e.* the eigenvalues of S_z (I_z) and s_z^A. This condition is automatically guaranteed for (**n**) by using easily available magnetic fields $B_0 \geq 0.1$ T, such that $g_z^A\mu_B B_0 \gg A_{x,y}$. As far as (**e**) is concerned, we require $J_{x,y}$ to be significantly smaller than the difference between excitation energies of the qudit $M \rightarrow M + 1$, and of the qubit, *i.e.*, $|J_{x,y}| \ll |(g_z - g_z^A)\mu_B B_0 + D(2M + 1)|$. This condition can also be fulfilled, by proper choice of the spin system and of the external field (see below).

As we explain in detail below, in both the electronic and nuclear systems, the spin 1/2 unit acts as an ancilla, exploited for detecting errors, while the $S, I > 1$ multi-level spin encodes the protected unit. All transitions between the eigenstates of $H_e(H_n)$ are theoretically addressable, thanks to the zero-field splitting (quadrupole) and interaction terms, which make all of them spectrally distinguishable. In practice, individually addressing each transition might be experimentally challenging, and we discuss below how proper choice of the pulse shape might help.

These transitions are driven by time-dependent magnetic fields $b_1(t)$ parallel to x, which couple to the system *via* the Hamiltonian

$$H_{1e} = \mu_B b_1(t)(g_x^A s_x^A + g_x S_x), \quad (3)$$

or

$$H_{1n} = b_1(t)(\mu_B g_x^A s_x^A + \mu_N g_N I_x) \quad (4)$$

for (**e**) and (**n**), respectively. The time evolution of (**e**) is computed by numerically solving the equation of motion for the system density matrix ρ:

$$\begin{aligned}\frac{d\rho(t)}{dt} &= -\frac{i}{\hbar}[H_e + H_{1e}(t), \rho(t)] \\ &+ \frac{1}{T_2}[2S_z\rho(t)S_z - S_z^2\rho(t) - \rho(t)S_z^2] \\ &+ \frac{1}{T_2^A}[2s_z^A\rho(t)s_z^A - s_z^{A2}\rho(t) - \rho(t)s_z^{A2}]\end{aligned} \quad (5)$$

and analogously for (**n**), by replacing $H_e(H_{1e})$ with $H_n(H_{1n})$ and S_z with I_z. Here the first line represents the coherent evolution, induced by the static, as well as time-dependent Hamiltonian terms, while the second and third ones describe pure dephasing on the qudit and on the ancilla, respectively, with dephasing times T_2 and T_2^A.

3 Results

3.1 Quantum-error correction with molecular spin qudits

Quantum systems are inherently fragile, because their interaction with the external environment tends to induce relaxation towards thermal equilibrium and to destroy quantum superpositions. However, to implement quantum computing algorithms and/or to store information in quantum memories, the state of the quantum register must be kept in superpositions of the Hamiltonian eigenstates for rather long times. Such states are particularly vulnerable. Hence, a strategy to overcome decoherence is mandatory to realize a reliable quantum computer. Quantum error correction provides a clear route towards this goal.

To give an intuitive picture of the working principles of a QEC code, we consider the elementary unit of a quantum computer, *i.e.* a qubit. This consists of a two-level quantum system, such as a spin 1/2, which can encode the two binary logical states $|0\rangle$ and $|1\rangle$. If we prepare the qubit in a generic superposition $\alpha|0\rangle + \beta|1\rangle$, the effect of unwanted errors is to corrupt the logical state, by changing the relative population of the two states and/or by inducing a decay of their coherence. In both cases, the information initially encoded into the complex coefficients α and β is deformed and cannot be recovered. This is because any error acts into the two-dimensional space which is already completely used to encode the logical state.

To make errors detectable, we need to extend the available space with the addition of some extra-levels. Intuitively, if errors bring the encoded superposition state rigidly into these extra levels (without altering α and β), then these errors can be detected and properly corrected. To achieve this, one needs to.

(1) identify the errors (or at least the leading ones) affecting the investigated system.

(2) Properly encode the logical states into code words $|0_L\rangle$ and $|1_L\rangle$, represented by superpositions of the Hamiltonian eigenstates. In particular, errors must have a symmetric effect on $|0_L\rangle$ and $|1_L\rangle$, bringing them rigidly outside from the computational space.

(3) Design a strategy to detect and correct errors without corrupting α and β.

The formalization of these concepts is given by Knill–Laflamnme conditions:[49] given a set of error operators $\{E_k\}$, logical states $|0_L\rangle$ and $|1_L\rangle$ enable error detection and correction if and only if the following identities hold:

$$\begin{aligned}\langle 0_L|E_k^\dagger E_j|1_L\rangle &= 0\\ \langle 0_L|E_k^\dagger E_j|0_L\rangle &= \langle 1_L|E_k^\dagger E_j|1_L\rangle.\end{aligned} \tag{6}$$

In other words, (i) different errors must not induce an overlap between the two code words and (ii) errors must act symmetrically on the two code words, in order not to distort the encoded superposition.

We now consider the application of these concepts to the concrete case under investigation: a spin S molecular system, as first proposed in ref. 44. At low temperature, the leading error is given by pure dephasing, originating from the interaction between the central spin and the surrounding nuclear spin bath.[45] To pinpoint the error operators E_k, we consider the effect of pure dephasing on the time evolution of the density matrix. This is expressed by the Lindblad equation (second line of eqn (6): $\dot{\rho} = 1/T_2(2S_z\rho S_z - {S_z}^2\rho - \rho {S_z}^2)$. The solution of this equation at time t can be expanded in series, $\rho(t) = \sum_k E_k\rho(0)E_k^\dagger$, with error operators

$$E_k = \sqrt{\frac{(2t/T_2)^k}{k!}}\mathrm{e}^{-S_z^2 t/T_2}S_z^k, \tag{7}$$

corresponding to powers of S_z. Hence, at short times, the dynamics is governed by low powers of S_z, while higher powers only enter at longer times. The first order error E_1 (for small t/T_2) is proportional to S_z. To correct this single error, which can already give a substantial gain in the effective coherence, four levels ($S = 3/2$) suffice. In particular, by choosing the code words

$$\begin{aligned}|0_L\rangle &= \frac{|3/2\rangle + \sqrt{3}|-1/2\rangle}{2}\\ |1_L\rangle &= \frac{\sqrt{3}|1/2\rangle + |-3/2\rangle}{2}\end{aligned} \tag{8}$$

one can easily check that, subject to an S_z error, they are transformed into

$$\begin{aligned}|e_0\rangle &= \frac{S_z|0_L\rangle}{||S_z|0_L\rangle||} = \frac{\sqrt{3}|3/2\rangle - |-1/2\rangle}{2}\\ |e_1\rangle &= \frac{S_z|1_L\rangle}{||S_z|1_L\rangle||} = \frac{|1/2\rangle - \sqrt{3}|-3/2\rangle}{2}\end{aligned} \tag{9}$$

which are orthogonal to both $|0_L\rangle$ and $|1_L\rangle$. This means that a generic encoded state $\alpha|0_L\rangle + \beta|1_L\rangle$ is transformed by the leading error into $\alpha|e_0\rangle + \beta|e_1\rangle$, without corrupting α and β. This allows us to discriminate between the correct and the wrong state and hence to design a sequence of pulses able to manage and correct this error (see below).

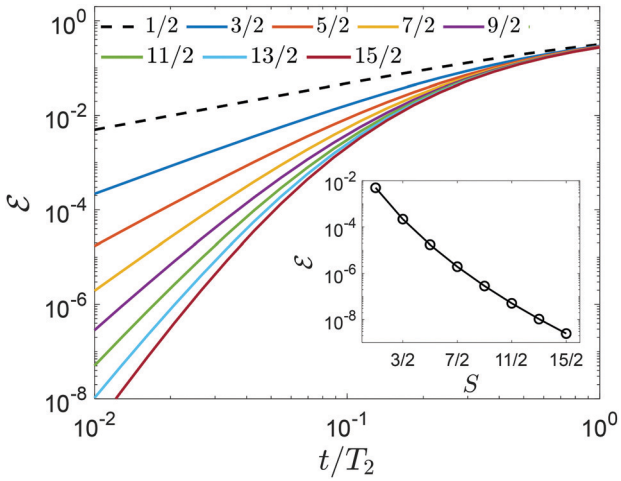

Fig. 1 Error $\mathscr{E}$ after QEC as a function of the memory time t (in units of T_2), for different values of S. In this simulation, the system is prepared in the state $|\psi_0\rangle = (|0_L\rangle + |1_L\rangle)/\sqrt{2}$ and evolves subject to pure dephasing for a time t. The capacity of the code increases with S, as shown in the inset for fixed $t/T_2 = 10^{-2}$.

By increasing the number of levels in the system, higher powers of S_z can also be corrected, thus in principle improving the capacity of the code.[44] This is shown in Fig. 1, where we report the error $\mathscr{E} = 1 - \langle\psi(0)|\rho(t)|\psi(0)\rangle$ after a memory time t, for a system initialized in $|\psi_0\rangle = (|0_L\rangle + |1_L\rangle)/\sqrt{2}$. At fixed t/T_2 (inset), we note that $\mathscr{E}$ decreases by increasing the number of levels in qudit levels, *i.e.* the spin S. In general, $2(n+1)$ levels (half for each logical state) are needed to distinguish (and hence possibly correct) n different errors. Otherwise, different errors overlap and correction becomes impossible.

We remark, however, that the actual corrective capability of the code is limited by the finite duration of the pulses needed to physically implement the correction. Indeed, during this step the system (which is not protected) accumulates errors arising from (i) leakage (*i.e.* unwanted transitions to neighboring levels, different from the addressed ones) and (ii) decoherence. Hence, a trade-off must be found between the gain obtained from QEC and the cost of actually implementing it, both increasing with the number of available levels.[44]

Having this in mind, we focus here on spin 3/2 qudit systems, which already ensure the possibility to correct the leading (first order) dephasing error (associated to S_z operator), while still limiting the complexity of the manipulations. This, together with the proper choice of the system (see next section), makes the proposal closer to possible experimental demonstrations.

Hereafter, we describe step by step the sequence of resonant pulses (see Fig. 2) that can be used to (i) encode the logical states (ii) detect the whether an S_z error has occurred or not and (iii) recover the initial state. Horizontal lines represent the eigenstates of the qudit Hamiltonian, labelled by the expectation value of $S_z(I_z)$. At the beginning of the sequence we prepare the ancilla in the $|\downarrow\rangle$ state and we store logic qubit information

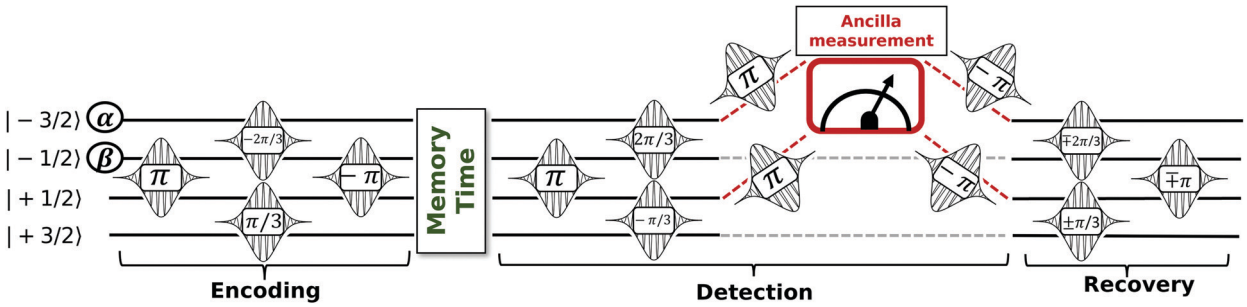

Fig. 2 Quantum error correction scheme to correct to first order pure dephasing, by using a four levels qudit system (coupled to an ancilla). Each horizontal line represents an eigenstate of the qudit Hamiltonian, with time increasing from left to right. The system is initialized with the ancilla in its ground $|\downarrow\rangle$ state and the logical qubit into the first top two levels. Gaussian symbols represent resonant magnetic pulses and their relative angles. The sequence is divided in three steps: encoding, detection and recovery. Second part of the detection step involves two of the states where ancilla is in $|\uparrow\rangle$ state. Red dashed lines represent conditional excitation (de-excitation) of ancilla. Recovery angles in the last part of the sequence depend on the results of ancilla measurement: we use top (down) sign if ancilla is in the $|\uparrow\rangle$ ($|\downarrow\rangle$) state.

in the first two top levels $|-3/2\rangle$ and $|-1/2\rangle$. The first step consists of four pulses (two of which in parallel) and implements the transformation $|-3/2\rangle \rightarrow |0_L\rangle$ and $|-1/2\rangle \rightarrow |1_L\rangle$, which encode the wavefunction into the protected logical state. We then let the system evolve freely during the memory time (only subject to decoherence). The next sequence of pulses is used to detect possible errors. We first decode information by mapping each of the four states $\{|0_L\rangle,|1_L\rangle, |e_0\rangle,|e_1\rangle\}$ to a different $|M\rangle$ state. This brings the correct superposition to $\alpha|-3/2\rangle + \beta|1/2\rangle$ and the wrong one to $\alpha|-1/2\rangle + \beta|3/2\rangle$. Thanks to the qudit-ancilla interaction, the excitation energy of the ancilla depends on the state of the qudit. We exploit this feature to conditionally excite the ancilla *via* two parallel π pulses corresponding to the qudit in states $|-3/2\rangle$ and $|1/2\rangle$. The corrupted and uncorrupted qudit states can now be easily distinguished by measuring the ancilla. Based on the measurement result, we then reconstruct the protected quantum information with the final sequence of three recovery pulses (with top/bottom sign of rotation angle depending if the ancilla was found to be $|\uparrow\rangle/|\downarrow\rangle$).

In the following we study the performance of the code on different, realistic systems and different forms of the driving field $b_1(t)$. Simulations are performed by numerically integrating eqn (5), with the system always subject to decoherence, even during the implementation of the pulses. Our aim is to find system-specific optimal working points to limit leakage and decoherence during the implementation of the whole error-correction procedure. Reducing the former requires long (frequency-selective) pulses, while to limit the latter one needs short pulses. Hence, a proper trade-off must be identified.

3.2 Physical implementations

In order to guide future synthetic efforts towards the first proof-of-principle experiments, the QEC scheme described above is applied to realistic model systems. We recall that the curves reported in Fig. 1 represent the ideal performance of the QEC code, as if correction pulses were (i) instantaneous, (ii) perfectly monochromatic and (iii) with the ancilla completely factorized from the qudit state.

These three conditions are not entirely satisfied in a real implementation and lead to different errors that are accounted for by our simulations:

(1) the finite duration of the pulses translates into decoherence occurring also during the QEC procedure, when the state is not encoded and hence the correction provided by the code is not active.

(2) The unavoidable presence of frequency components slightly different from the leading one induces leakage to levels others than those addressed by each pulse.

(3) The mixing between qudit and ancilla wavefunctions is induced by transverse components of the coupling ($J_{x,y}$) and yields a measurement error during the detection step of Fig. 2. This means there is a finite probability of finding ancilla $|\downarrow\rangle$ even when no error had occurred and *vice versa*.

All of these imperfections yield a plateau in the final error $\mathscr{E}$ at short t/T_2, appearing in both Fig. 3b and 4b, at odds with Fig. 1. For large t/T_2, the performance of the code approaches the ideal situation. We now discuss the effect of these different imperfections in the two test-cases under investigation, whose parameters are listed in Table 1.

3.2.1 Electronic spin qudit. First, we consider two hypothetical dimers consisting of an electronic Cr^{3+} $S = 3/2$ ion, weakly coupled to an (effective) spin 1/2. We assume realistic parameters for a Cr^{3+} ion in an octahedral crystal field, *i.e.* $D = -0.24$ cm^{-1} and an isotropic $g = 1.98$. In order to ensure factorization between qudit and ancilla states, we need $|(g - g_z^A)\mu_B B_0 + D(2M + 1)| \gg |J_{x,y}|$. We consider two possible candidates for the role of ancilla, namely Cu^{2+} and Yb^{3+} complexes. The possibility to synthesize CrCu dimers (**e1** hereafter) has been recently discussed in ref. 36, while a possible CrYb dimer (**e2** from now on) already exists.[50] Typical parameters for Cu^{2+} are $g_z^A = 2.3$ and $g_x^A = 2.1$ (see, for instance, ref. 12) while for Yb^{3+} $g_z^A = 4.2$ and $g_x^A = 2.9$, as reported in ref. 51 for an Yb(trensal) complex. We assume an axially anisotropic exchange interaction with $J_x = J_y = 1.7 \times 10^{-2}$ cm^{-1} and $J_z = -3.3 \times 10^{-2}$ cm^{-1}, as one could obtain with a dipole–dipole coupling, by placing the two ions 5–6 Å apart. The energy level diagram for CrYb is reported in Fig. 3a as a function of the external field, with the eigenstates indicated on the right.

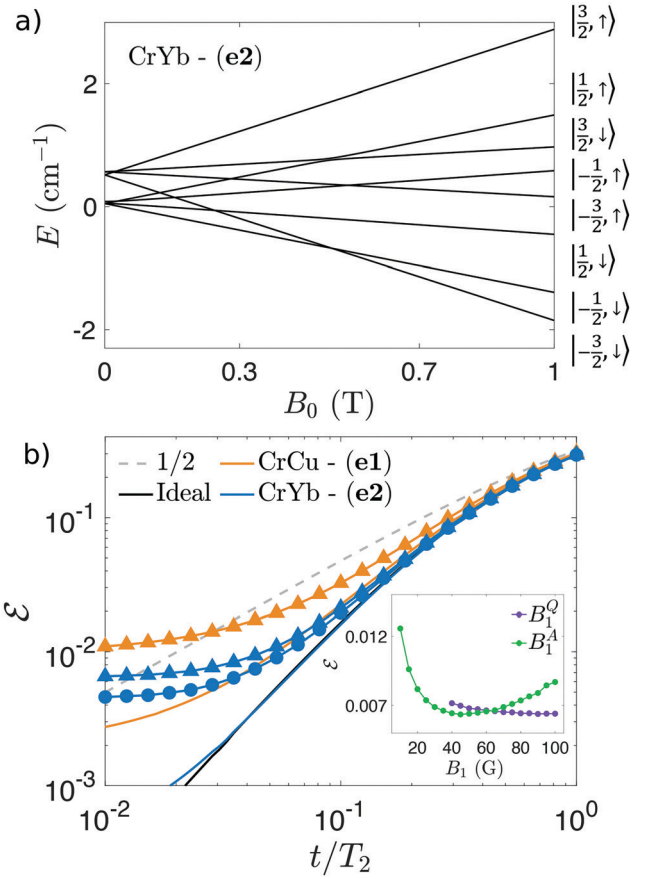

Fig. 3 (a) Energy levels as function of the static field B_0 for the (**e2**) system,[50] with the practically factorized states labelled by S_z and s_z^A expectation values. (b) Comparison between (**e1**) and (**e2**) implementations of the QEC scheme. The grey dashed line represents the error for an uncorrected s = 1/2 spin subject to decoherence. The continuous black line is the ideal performance of QEC scheme on a S = 3/2 qudit. Solid orange (blue) line are measurement errors for (**e1**) ((**e2**)) using B_1^Q = 100 G and B_1^A = 45 G at B_0 = 1 T. Corresponding symbols are simulations including also decoherence and leakage errors. For (**e2**) dimer we show results using two possible values of T_2^A: 1 μs (triangles) and 3 μs (circles). Inset: Total error as a function of the amplitude of the Gaussian driving field for qudit (violet) and ancilla (green) excitations on (**e2**), for fixed t/T_2 = 0.035, T_2 = 50 μs and T_2^A = 3 μs.

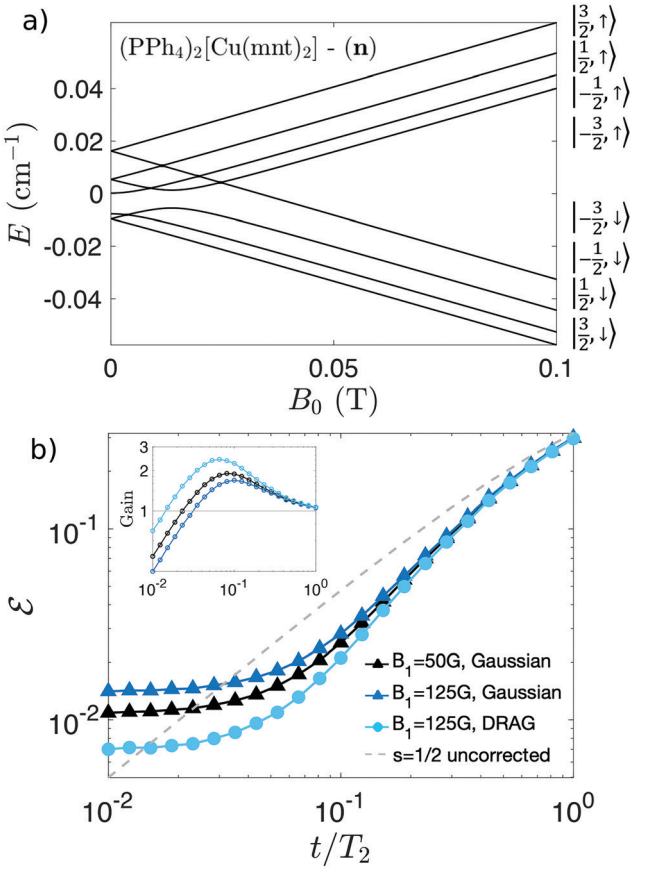

Fig. 4 (a) Energy levels of $(PPh_4)_2[Cu(mnt)_2]$ **n**, consisting of a Cu^{2+} ion (electronic spin s^A = 1/2), coupled to the nuclear I = 3/2 spin by hyperfine interaction (as reported in ref. 28), as function of the external field B_0. The composition of the eigenstates is indicated on the right. (b) Symbols: error after implementation of the QEC scheme with T_2 = 0.5 ms, B_0 = 0.1 T, T_2^A = 68 μs (as reported in ref. 28), B_1^A = 30G, with different forms of the driving fields B_1^Q: Gaussian (triangles) and DRAG (circles). Dashed grey line: error for an uncorrected s = 1/2 spin due to decoherence. Inset: Corresponding gain, *i.e.* ratio between errors on an uncorrected qubit and on a protected system.

The performance of the QEC, quantified by the error $\mathcal{E}$, is reported in panel (b), as a function of the memory time.

The measurement error arising from imperfect factorization deserves a preliminary discussion. To highlight its importance and disentangle it from other errors, we report by solid coloured lines the final error obtained with ideal pulses, but measurement operators resulting from diagonalization of the system Hamiltonian, thus including small qudit-ancilla entanglement. At fixed B_0 = 1 T, $\mathcal{E}$ is significantly larger for (**e1**), due the smaller $g_z^A - g_z$, and sets a lower limit to the accuracy of the whole procedure. In the case of (**e2**), factorization is much higher (see blue solid curve in Fig. 3) and the final error can be neglected, compared to leakage and decoherence. Clearly, a similar situation could be achieved for (**e1**) by increasing B_0.

We now turn our attention to errors due to leakage and decoherence. In the simulations reported in this section, we use Gaussian shaped pulses, $b_1(t) = B_1 e^{-(t-t_0)^2/2\tau^2} \cos \omega t$, choosing ω for each pulse to be in resonance with the pair of energy levels coupled by the corresponding transition indicated in Fig. 2. We find that leakage is practically irrelevant when addressing qudit transitions. Indeed, thanks to the large difference between energy gaps ensured by D, we can safely employ B_1 up to 100 G without significantly transfer population to unwanted states. This is demonstrated in the inset of Fig. 3b, where we show $\mathcal{E}$ at fixed t/T_2, as a function of B_1^Q (the amplitude of the driving field used for qudit transitions). We note that $\mathcal{E}$ is monotonically decreasing with B_1^Q. This means that by shortening the pulses we gain further and further and hence that the total error is limited by decoherence. We thus fix B_1^Q = 100 G, as provided state-of-the-art pulse electron-paramagnetic resonance technology.[52] Conversely, excitations of the ancilla (depending on the qudit state) are resolved by J_z and hence the corresponding transitions are

Table 1 Parameters used in the simulations for (**e**) and (**n**), a hypothetical CrCu/CrYb dimer[50] and typical of a ^{63}Cu ion (see, *e.g.*, ref. 28). We assume **J** as a diagonal tensor with diagonal components J_α (and similarly for A and g^A), while the qudit's g is isotropic

	g	D/Q (cm^{-1})	$(J_x, J_y, J_z)/(A_x, A_y, A_z)$ (cm^{-1})	(g_x^A, g_y^A, g_z^A)	T_2 (μs)	T_2^A (μs)
CrCu (**e1**)	1.98	−0.24	$(1.7, 1.7, -3.3) \times 10^{-2}$	(2.1, 2.1, 2.3)	50	5
CrYb (**e2**)				(2.9, 2.9, 4.2)	50	1–3
$(PPh_4)_2$ [Cu(mnt)$_2$] (**n**)	1.48	1.7×10^{-3}	$(0.4, 0.4, 1.7) \times 10^{-2}$	(2.0, 2.0, 2.1)	10^2–10^3	68

closer in energy. Hence, a smaller amplitude of the oscillating field (B_1^A) must be chosen, in order to reduce leakage. This optimal value is set by the position of the minimum of $\mathscr{E}$ as a function of B_1^A ($\sim$45 G), reported again in the inset of Fig. 3b. For B_1^A smaller than the optimal working point pulses are frequency selective but rather long, and hence decoherence dominates. Above the minimum, pulses are shorter but broader in frequency, and hence leakage becomes more important.

The resulting simulations, using the optimal values of B_1^Q and B_1^A, are shown by symbols in Fig. 3b, with T_2 = 50 μs. This is a rather optimistic value, but within the range of attainable coherence times for transition metal complexes with properly engineered ligand cage.

The performance of (**e1**) dimer (orange triangles) is mainly limited by the measurement error discussed above, which is negligible for (**e2**) (blue symbols). As far as T_2^A is concerned, we can safely assume a value significantly smaller than T_2, because the ancilla is only excited during the error-detection step, while it is kept in its ground state for most of the time. Nevertheless, we find T_2^A relevant to determine the final performance of the code. We used 5 μs for (**e1**) and 1 μs for (**e2**), as found in ref. 51. By increasing T_2^A from 1 to 3 μs (blue circles), the total error is further reduced (see blue triangles *vs.* circles), reaching values below 5×10^{-3} at short times.

3.2.2 Nuclear spin qudit. As far as (**n**) is concerned, we consider an existing molecule, namely $(PPh_4)_2$ [Cu(mnt)$_2$] reported in ref. 28, which contains a Cu^{2+} ion (electronic spin s^A = 1/2), coupled to the nuclear I = 3/2 spin by hyperfine interaction $A = (0.4,0.4,1.7) \times 10^{-2}$ cm^{-1}. A crucial parameter is represented by the nuclear quadrupole coupling Q, which sets the energy resolution between adjacent nuclear spin transitions, not measured in the electron paramagnetic resonance study reported in ref. 28. For the ^{63}Cu isotope, a reasonable choice is $Q = 1.7 \times 10^{-3}$ cm^{-1}.[53,54] The energy levels as a function of the applied magnetic field are shown in Fig. 4a, with the two subspaces corresponding to the two different states of the ancilla ($|\downarrow\rangle$ and $|\uparrow\rangle$) clearly separated. Only the former represent the encoding subspace, while the latter is only involved in the detection step of Fig. 2.

In the simulations reported below, we use B_0 = 0.1 T, in order to exploit the small mixing between electronic and nuclear spin wave function to speed-up nuclear manipulations. Indeed, this optimal value of B_0 allows us to both keep the eigenstates factorized, while enhancing by $\sim$50 the matrix element of nuclear transitions.[55,56]

Thanks to the large difference between electronic and nuclear excitation energies, factorization here is not an issue, having a maximum states mixing of 10^{-3}. We can therefore focus on errors due to decoherence and leakage. As far as the nuclear coherence time T_2 is concerned, we do not have experimental data at hand. However, a reasonable estimate can be done by comparison with similar systems, consisting of hyperfine-coupled electronic and nuclear spins. At the rather low fields considered here, decoherence of the central qudit is induced by the coupling with the surrounding magnetic nuclei, primarily mediated by the electronic spin component of the system state. Hence, the nuclear T_2 is directly related to the electronic one and is found to be at least ten times larger in recent studies on Yb(trensal) and vanadyl tetraphenylporphyrinate.[12,55] The latter consists of a spin 1/2 electronic spin coupled to a I = 7/2 nucleus, with hyperfine interaction very similar to $(PPh_4)_2$-[Cu(mnt)$_2$] and hence represents an optimal benchmark. Here, given the remarkably long value measured for T_2^A at 5 K (68 μs), it is reasonable to first assume, for the associated nuclear qudit, T_2 = 0.5 ms. In addition, we set B_1^Q = 50 G and B_1^A = 30 G. The resulting final error is shown in Fig. 4 by black triangles, while the inset reports the corresponding gain, *i.e.* the ratio between the error on a not-protected qubit (dashed line) and that on the protected qudit. The maximum gain reaches values close to 2. To improve it, one could try to increase B_1. Larger values of the driving field amplitude would reduce the duration of the sequence (and hence the impact of decoherence), at the price of increasing leakage to neighboring levels. This harmful effect is dominant for B_1^Q = 125 G, as evidenced by the increase of from black and blue triangles in Fig. 4b. Hence, faster sequences require proper pulse-shaping techniques, as illustrated in the next section.

3.3 Pulse engineering to improve the performance of the code: DRAG

We investigate here pulse-shaping techniques to speed up pulses as much as possible while still keeping leakage under control. This will reduce the effect of decoherence during the implementation of QEC, when the system is not protected.

The goal is particularly challenging when the difference between the gaps is similar to the spectral width of the pulse.

Several techniques exist to minimize leakage while using rather short pulses, such as Sideband Modulation (WhaWha: anharmonicity with average Hamiltonian)[57,58] and the SWIPHT (speeding up wave forms by inducing phases to harmful transitions).[59,60] Here we focus on the *derivative removal by adiabatic gate* (DRAG), which allows us to get high-fidelity two-level rotations with significant gate speedups.[48,61,62] The main idea behind DRAG is that a second control pulse that is the time derivative of the first creates a spectral hole. Then, by adjusting the time-derivative pulse, the spectral hole can be moved close to the unwanted transition, thereby minimizing

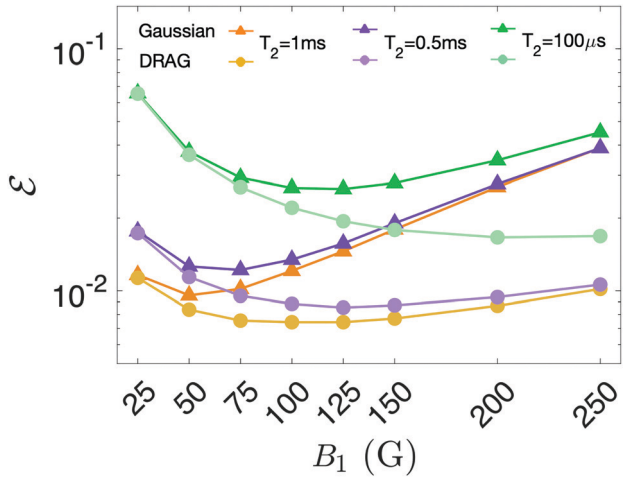

Fig. 5 Effect of DRAG on the error after QEC on system (**n**) as a function of B_1, for different values of T_2. Computations are performed on a t/T_2 near to the maximum gain, as reported in Fig. 4 inset. Dark (light) lines refer to Gaussian (DRAG) pulses, while different colours represent different values of T_2. The advantage of DRAG is maximum at intermediate B_1 for long T_2 and moves to larger B_1 by decreasing T_2.

leakage to a third level, as shown in the inset of Fig. 5. More specifically, the driving field assumes the form:

$$b_1(t) = \begin{cases} \varepsilon_x(t)\cos\omega_d t + \varepsilon_y(t)\sin\omega_d t & 0 < t < t_g \\ 0 & \text{otherwise} \end{cases} \quad (10)$$

that is a single frequency carrier with two independent quadrature controls. In a DRAG scheme, using Gaussian-shaped pulses as the main driving field, the x and y channels are described by:

$$\begin{aligned} \varepsilon_x(t) &= B_1 e^{-(t-t_0)^2/2\tau^2}, \\ \varepsilon_y(t) &= \beta\lambda\frac{d\varepsilon_x(t)}{dt}, \end{aligned} \quad (11)$$

where B_1 is the maximum pulses amplitude, fixed by the rotation angle we want to implement, λ is a parameter accounting for the relative strength between the unwanted and the desired transition and β is a parameter (also depending on the addressed transition and operation), which we obtain in the following by numerical optimization.

In its simplest implementation, DRAG method works well when a unique transition disturbs the selected one. Hence, we have applied this technique only to qudit transitions (B_1^Q) of the (**n**) system, to distinguish transitions $|3/2\rangle \leftrightarrow |1/2\rangle$ and $|-1/2\rangle \leftrightarrow |-3/2\rangle$ from $|1/2\rangle \leftrightarrow |-1/2\rangle$. In the case of excitations of the ancilla, we usually have two gaps close to the selected transitions.

The advantage of DRAG is clear when we use fast pulses and we consider a system with similar energy gaps. Indeed, in this regime the difference between the gaps is comparable to the width of the pulse and hence the leakage becomes an issue.

We compare in Fig. 5 the performance of the code by using simple Gaussian or DRAG pulses, as a function of B_1 and for different values of T_2, computed near the t/T_2 maximum gain, as reported in Fig. 4 inset. To clearly highlight the effect of proper pulse-shaping, we investigate regimes even employing magnetic field amplitudes larger than those available in current experimental apparatus (close to 120 G for pulse nuclear magnetic resonance experiments[63]). The aim is to guide future technological developments in this direction.

Results are shown in Fig. 5, with dark (light) curves referred to Gaussian (DRAG) pulses and different colours indicating different values of T_2. In all the examined cases, the use of Gaussian driving pulses leads to a minimum in $\mathscr{E}$ at intermediate B_1. Below this minimum value, pulse length is the limiting factor and hence decoherence is the leading error. For larger B_1 (*i.e.* shorter pulses), above the minimum, the final accuracy is substantially limited by leakage, due to the fact that pulses become less monochromatic. By increasing T_2, the effect of decoherence is reduced and hence the minimum moves to lower values of B_1. In the infinite T_2 limit, $\mathscr{E}$ becomes monotonically increasing with B_1. The reduction of leakage by application of the DRAG method is clearly evidenced by the reduction of the slope of $\mathscr{E}$ above the minimum. For $T_2 = 100$ μs the minimum is above 250 G, and its position is (again) lowered by increasing T_2. However, compared to the case of Gaussian pulses, the increase of $\mathscr{E}$ with B_1 remains much weaker. Hence, application of the DRAG technique significantly improves the overall performance of the QEC code.

3.4 Single-qubit gates on encoded states

Here we present a scheme to implement single-qubit gates on encoded states, such as $R_z(\vartheta)$ and $R_y(\vartheta)$ rotations of an arbitrary angle ϑ. By combining them, a generic single-qubit operation can be obtained. For instance, the Hadamard gate (involved in many quantum algorithms) results from $R_z(\pi)R_y(\pi/2)$.

Our aim is to design a strategy which exploits transitions between energy levels while keeping the states encoded as much as possible. Reducing the amount of time the system is un-encoded helps to limit the effect of decoherence while the system is not protected.

The effect of a $R_z(\vartheta)$ gate consists in adding a relative phase between $|0_L\rangle$ and $|1_L\rangle$, *i.e.* implementing the transformation

$$\begin{aligned} R_Z(\vartheta)|\psi\rangle &= \alpha|0_L\rangle + \beta e^{i\vartheta}|1_L\rangle = \\ &= \frac{\alpha}{2}\left(|3/2\rangle + \sqrt{3}|-1/2\rangle\right) + \frac{\beta}{2}e^{i\vartheta}\left(|-3/2\rangle + \sqrt{3}|1/2\rangle\right). \end{aligned} \quad (12)$$

This can be achieved by exploiting two semi-resonant excitations of the ancilla for the two states entering the definition of $|1_L\rangle$, namely $|-3/2\rangle$ and $|1/2\rangle$. Semi-resonant excitations are obtained by a π pulse with a frequency detuned by a small amount δ_{ij} from the addressed energy gap. In particular, a rectangular semi-resonant pulse of duration $\Delta t = \pi/\sqrt{G_{ij}^2 + \delta_{ij}^2/4}$ adds a phase $\vartheta = \pi - \pi\left[\delta_{ij}/\sqrt{\delta_{ij}^2 + 4G_{ij}^2}\right]$ to the system wave function, with G_{ij} the matrix element of the transition.[64] By employing only excitations of the ancilla, this scheme allows us to implement the $R_z(\vartheta)$ gate without ever

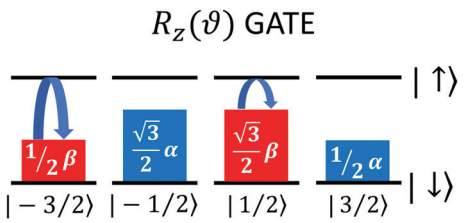

Fig. 6 Scheme to implement a protected R_z gate on a S = 3/2 qudit, encoding a protected qubit. Top (bottom) levels correspond to ↑ (↓) states of the ancilla, while different colours indicate components of the wavefunction on different $|0_L\rangle/|1_L\rangle$ logical states. The scheme exploits semi-resonant pulses (arrows) of the two states entering the definition of $|1_L\rangle$.

decoding quantum information stored in the qudit, which therefore remains protected from dephasing (Fig. 6).

$R_{x,y}(\vartheta)$ rotations are more tricky. Indeed, they necessarily involve population transfer between energy levels (such as ±3/2) which are not directly connected by $H_{1e,n}$. Hence, the implementation of logical $R_{x,y}(\vartheta)$ gates on a spin S qudit requires a decomposition into several pulses, which in turn implies to leave the protected code-space for some time. To limit this time as much as possible, one could for instance exploit excitations of the ancilla to manipulate in parallel ±3/2 and ±1/2 components of the qudit state.

4 Discussion and conclusions

To sum up, we have shown the performance of two realistic molecular spin qudits as protected logical units for quantum computation, embedding quantum error correction against pure dephasing, the leading error in this class of systems.

We have investigated by extensive numerical simulations the improvement in the final error after implementation of a targeted quantum error correction procedure, compared to an uncorrected qubit. Our study has focused on two different implementations, based on an existing nuclear spin 3/2 qudit, coupled to an electronic ancilla by hyperfine interaction, and on a hypothetical (but realistic) electronic spin dimer, where a S = 3/2 qudit encodes quantum information, while an effective spin 1/2 plays the role of ancilla. The latter is used to detect errors without corrupting quantum information stored into the qudit degrees of freedom. We deeply investigate different sources of error which limit the performance of the code and we identify the proper range of couplings and coherence times allowing us to achieve a good protection. In addition, we study the dependence of our results on the form of the driving field, we find system-specific optimal working points and we apply pulse-shaping techniques to reduce the length of the pulses, while keeping leakage under control. In both the electronic and the nuclear case, we reach residual errors significantly lower than 10^{-2}. We note, in turn, that optimal quantum control methods could be applied to further reduce leakage to neighboring levels and pulse length, as recently shown in ref. 65. Finally, multi-spin molecules with small total spin but a large connectivity between energy levels could be used,[66,67] thus potentially speeding-up manipulations.

Being based on realistic choices of the experimental parameters, our results indicate a clear route to guide the synthesis of molecules for future proof-of-concepts experiments.

Conflicts of interest

There are no conflicts to declare.

Acknowledgements

This work has received funding from the European Unions Horizon 2020 research and innovation programme (FET-OPEN project FATMOLS) under grant agreement no. 862893.

Notes and references

1 A. Chiesa, G. F. S. Whitehead, S. Carretta, L. Carthy, G. A. Timco, S. J. Teat, G. Amoretti, E. Pavarini, R. E. P. Winpenny and P. Santini, *Sci. Rep.*, 2014, **4**, 7423.
2 D. Aguilà, D. Barrios, V. Velasco, O. Roubeau, A. Repollés, P. Alonso, J. Sesé, S. Teat, F. Luis and G. Aromí, *J. Am. Chem. Soc.*, 2014, **136**, 14215.
3 A. Ardavan, A. M. Bowen, A. Fernandez, A. J. Fielding, D. Kaminski, F. Moro, C. A. Muryn, M. D. Wise, A. Ruggi, E. J. L. McInnes, K. Severin, G. A. Timco, C. R. Timmel, F. Tuna, G. F. S. Whitehead and R. E. P. Winpenny, *npj Quantum Inf.*, 2015, **1**, 15012.
4 J. Ferrando-Soria, E. Moreno-Pineda, A. Chiesa, A. Fernandez, S. A. Magee, S. Carretta, P. Santini, I. Vitorica-Yrezabal, F. Tuna, E. J. L. McInness and R. E. P. Winpenny, *Nat. Commun.*, 2016, **7**, 11377.
5 M. Atzori, L. Tesi, E. Morra, M. Chiesa, L. Sorace and R. Sessoli, *J. Am. Chem. Soc.*, 2016, **138**, 2154–2157.
6 M. Atzori, E. Morra, L. Tesi, A. Albino, M. Chiesa, L. Sorace and R. Sessoli, *J. Am. Chem. Soc.*, 2016, **138**, 11234–11244.
7 E. Moreno-Pineda, C. Godfrin, F. Balestro, W. Wernsdorfer and M. Ruben, *Chem. Soc. Rev.*, 2018, **47**, 501–513.
8 E. Macaluso, M. Rubín, D. Aguilà, A. Chiesa, J. I. M. L. A. Barrios, P. J. Alonso, O. Roubeau, F. Luis, G. Aromí and S. Carretta, *Chem. Sci.*, 2020, **11**, 10337.
9 A. Gaita-Ariño, F. Luis, S. Hill and E. Coronado, *Nat. Chem.*, 2019, **11**, 301.
10 M. Atzori and R. Sessoli, *J. Am. Chem. Soc.*, 2019, **141**, 11339.
11 C. Bonizzoni, A. Ghirri, F. Santanni, M. Atzori, L. Sorace, R. Sessoli and M. Affronte, *npj Quantum Inf.*, 2020, **6**, 68.
12 S. J. Lockyer, A. Chiesa, G. A. Timco, E. J. L. McInnes, T. S. Bennett, I. J. Vitorica-Yrezebal, S. Carretta and R. E. P. Winpenny, *Chem. Sci.*, 2021, **12**, 9104.
13 S. Carretta, D. Zueco, A. Chiesa, A. Gómez-León and F. Luis, *Appl. Phys. Lett.*, 2021, **118**, 240501.
14 S. Nakazawa, S. Nishida, T. Ise, T. Yoshino, N. Mori, R. D. Rahimi, K. Sato, Y. Morita, K. Toyota, D. Shiomi, M. Kitagawa, H. Hara, P. Carl, P. Höfer and T. Takui, *Angew. Chem., Int. Ed.*, 2012, **51**, 9860–9864.

15 S. Yamamoto, S. Nakazawa, K. Sugisaki, K. Sato, K. Toyota, D. Shiomi and T. Takui, *Phys. Chem. Chem. Phys.*, 2015, **17**, 2742–2749.
16 B. K. Rugg, M. D. Krzyaniak, B. T. Phelan, M. A. Ratner, R. M. Young and M. R. Wasielewski, *Nat. Chem.*, 2019, **11**, 981–986.
17 M. D. E. Wasielewski, M. R. Forbes, N. L. Frank, K. Kowalski, G. D. Scholes, J. Yuen-Zhou, M. A. Baldo, D. E. Freedman, R. H. Goldsmith, T. Goodson, M. L. Kirk, J. P. McCusker, J. K. Ogilvie, D. A. Shultz, S. Stoll and K. B. Whaley, *Nat. Rev. Chem.*, 2020, **4**, 490–504.
18 C. D. Bruzewicz, J. Chiaverini, R. McConnell and J. M. Sage, *Appl. Phys. Lett.*, 2019, **6**, 021314.
19 F. Tacchino, A. Chiesa, S. Carretta and D. Gerace, *Adv. Quantum Technol.*, 2019, **3**, 1900052.
20 I. Pogorelov, T. Feldker, C. D. Marciniak, L. Postler, G. Jacob, O. Krieglsteiner, V. Podlesnic, M. Meth, V. Negnevitsky, M. Stadler, B. Höfer, C. Wächter, K. Lakhmanskiy, R. Blatt, P. Schindler and T. Monz, *PRX Quantum*, 2021, **2**, 020343.
21 A. Chiesa, F. Tacchino, M. Grossi, P. Santini, I. Tavernelli, D. Gerace and S. Carretta, *Nat. Phys.*, 2019, **15**, 455.
22 F. Arute, *et al.*, *Nature*, 2019, **574**, 505.
23 F. Arute, *et al.*, *Science*, 2020, **369**, 1084.
24 P. Jurcevic, A. Javadi-Abhari, L. S. Bishop, I. Lauer, D. F. Bogorin, M. Brink, L. Capelluto, O. Günlük, T. Itoko, N. Kanazawa, A. Kandala, G. A. Keefe, K. Krsulich, W. Landers, E. P. Lewandowski, D. T. McClure, G. Nannicini, A. Narasgond, H. M. Nayfeh, E. Pritchett, M. B. Rothwell, S. Srinivasan, N. Sundaresan, C. Wang, K. X. Wei, C. J. Wood, J.-B. Yau, E. J. Zhang, O. E. Dial, J. M. Chow and J. M. Gambetta, *Quantum Sci. Technol.*, 2021, **6**, 025020.
25 A. Blais, A. L. Grimsmo, S. M. Girvin and A. Wallraff, *Rev. Mod. Phys.*, 2021, **93**, 025005.
26 A. Chatterjee, P. Stevenson, S. De Franceschi, A. Morello, N. P. de Leon and F. Kuemmeth, *Nat. Rev. Phys.*, 2021, **3**, 157–177.
27 Y.-S. Ding, Y.-F. Deng and Y.-Z. Zheng, *Magnetochemistry*, 2016, **2**, 40.
28 K. Bader, D. Dengler, S. Lenz, B. Endeward, S.-D. Jiang, P. Neugebauer and J. van Slageren, *Nat. Commun.*, 2014, **5**, 5304.
29 J. M. Zadrozny, J. Niklas, O. G. Poluektov and D. E. Freedman, *ACS Cent. Sci.*, 2015, **1**, 488.
30 M. Shiddiq, D. Komijani, Y. Duan, A. Gaita-Ariño, E. Coronado and S. Hill, *Nature*, 2016, **531**, 348.
31 M. Fataftah, J. M. Zadrozny, S. C. Coste, M. J. Graham, D. M. Rogers and D. E. Freedman, *J. Am. Chem. Soc.*, 2016, **138**, 1344.
32 M. K. Wojnar, D. W. Laorenza, R. D. Schaller and D. E. Freedman, *J. Am. Chem. Soc.*, 2020, **142**, 14826–14830.
33 J. Zadrozny and D. E. Freedman, *Inorg. Chem.*, 2015, **54**, 12027–12031.
34 Y. Wang, Z. Hu, B. C. Sanders and S. Kais, *Front. Phys.*, 2020, **8**, 479.
35 C. Cafaro, F. Maiolini and S. Mancini, *Phys. Rev. A: At., Mol., Opt. Phys.*, 2012, **86**, 022308.
36 F. Tacchino, A. Chiesa, R. Sessoli, I. Tavernelli and S. Carretta, *J. Mater. Chem. C*, 2021, **9**, 10266.
37 C. Godfrin, A. Ferhat, R. Ballou, S. Klyatskaya, M. Ruben, W. Wernsdorfer and F. Balestro, *Phys. Rev. Lett.*, 2017, **119**, 187702.
38 B. Mischuck and K. Mølmer, *Phys. Rev. A: At., Mol., Opt. Phys.*, 2013, **87**, 022341.
39 E. O. Kiktenko, A. K. Fedorov, O. V. Man'ko and V. I. Man'ko, *Phys. Rev. A: At., Mol., Opt. Phys.*, 2015, **91**, 042312.
40 P. Imany, J. A. Jaramillo-Villegas, M. S. Alshaykh, J. M. Lukens, O. D. Odele, A. J. Moore, D. E. Leaird, M. Qi and A. M. Weiner, *npj Quantum Inf.*, 2019, **5**, 59.
41 E. Kiktenko, A. Fedorov, A. Strakhov and V. Man'ko, *Phys. Lett. A*, 2015, **379**, 1409.
42 S. J. Devitt, W. J. Munro and K. Nemoto, *Rep. Progr. Phys.*, 2013, **76**, 076001.
43 B. M. Terhal, *Rev. Mod. Phys.*, 2015, **87**, 307.
44 A. Chiesa, E. Macaluso, F. Petiziol, S. Wimberger, P. Santini and S. Carretta, *J. Phys. Chem. Lett.*, 2020, **11**, 8610.
45 F. Petiziol, A. Chiesa, S. Wimberger, P. Santini and S. Carretta, *npj Quantum Inf.*, 2021, **7**, 133.
46 A. Chiesa, F. Petiziol, E. Macaluso, S. Wimberger, P. Santini and S. Carretta, *AIP Adv.*, 2021, **11**, 025134.
47 M. Werninghaus, D. J. Egger, F. Roy, S. Machnes, F. K. Wilhelm and S. Filipp, *npj Quantum Inf.*, 2021, **7**, 14.
48 J. M. Gambetta, F. Motzoi, S. T. Merkel and F. K. Wilhelm, *Phys. Rev. A: At., Mol., Opt. Phys.*, 2011, **83**, 012308.
49 E. Knill and R. Laflamme, *Phys. Rev. A: At., Mol., Opt. Phys.*, 1997, **55**, 900–911.
50 T. Sanada, T. Suzuki, T. Yoshida and S. Kaizaki, *Inorg. Chem.*, 1998, **37**, 4712.
51 K. S. Pedersen, A.-M. Ariciu, S. McAdams, H. Weihe, J. Bendix, F. Tuna and S. Piligkos, *J. Am. Chem. Soc.*, 2016, **138**, 5801–5804.
52 P. A. S. Cruickshank, D. R. Bolton, D. A. Robertson, R. I. Hunter, R. J. Wylde and G. M. Smith, *Rev. Sci. Instrum.*, 2009, **80**, 103102.
53 M. Fujii, F. Wakai, H. Abe and A. Hirai, *J. Phys. Soc. Jpn.*, 1981, **50**, 1109.
54 C. Mazzoli, G. Allodi, G. Guidi, R. De Renzi and P. Ghigna, *J. Magn. Magn. Mater.*, 2004, **272**, 106.
55 R. Hussain, G. Allodi, A. Chiesa, E. Garlatti, D. Mitcov, A. Konstantatos, K. Pedersen, R. D. Renzi, S. Piligkos and S. Carretta, *J. Am. Chem. Soc.*, 2018, **140**, 9814.
56 S. Chicco, A. Chiesa, G. Allodi, E. Garlatti, M. Atzori, L. Sorace, R. De Renzi, R. Sessoli and S. Carretta, *Chem. Sci.*, 2021, **12**, 12046.
57 R. Schutjens, F. A. Dagga, D. J. Egger and F. K. Wilhelm, *Phys. Rev. A: At., Mol., Opt. Phys.*, 2013, **88**, 052330.
58 L. S. Theis, F. Motzoi and F. K. Wilhelm, *Phys. Rev. A*, 2016, **93**, 012324.
59 S. P. Premaratne, J.-H. Yeh, F. C. Wellstood and B. S. Palmer, *Phys. Rev. A*, 2019, **99**, 012317.
60 S. E. Economou and E. Barnes, *Phys. Rev. B: Condens. Matter Mater. Phys.*, 2015, **91**, 161405.

61 F. Motzoi, J. M. Gambetta, P. Rebentrost and F. K. Wilhelm, *Phys. Rev. Lett.*, 2009, **103**, 110501.
62 A. De, *Quantum Inf. Process.*, 2019, **18**, 165.
63 K. J. Sanders, A. J. Pell, S. Wegner, C. P. Grey and G. Pintacuda, *Chem. Phys. Lett.*, 2018, **697**, 29.
64 A. Chiesa, P. Santini and D. A. Gerace, *Sci. Rep.*, 2015, **5**, 16036.
65 A. Castro, A. G. Carrizo, D. Zueco and F. Luis, **https://arxiv.org/abs/2111.15313**.
66 L. M. Baker, *et al.*, *Chem. – Eur. J.*, 2016, **22**, 1779–1788.
67 R. J. Woolfson, G. A. Timco, A. Chiesa, I. J. Vitorica-Yrezabal, F. Tuna, T. Guidi, E. Pavarini, P. Santini, S. Carretta and R. E. P. Winpenny, *Angew. Chem., Int. Ed.*, 2016, **55**, 8856–8859.